Research Article

Sayed Abdel-Khalek*, Mariam Algarni, and Kamal Berrada

Quantum resources for a system of two atoms interacting with a deformed field in the presence of intensity-dependent coupling

https://doi.org/10.1515/phys-2025-0163
received September 23, 2024; accepted April 28, 2025

Abstract: This study explores the dynamics of a two two-level atomic system interacting with a parity-deformed field, modeled as a coherent state. By varying the parity deformation parameter and incorporating the effects of intensity-dependent coupling, we examine the time evolution of key quantum phenomena. These include atomic population inversion, von Neumann entropy, concurrence, quantum Fisher information, and the Mandel parameter, where each serves as a critical indicator. Our analysis reveals how the interplay between the deformation parameter and coupling effects governs the quantum dynamics, influencing entanglement, parameter estimation, and statistical properties of the field. These insights contribute to a more comprehensive understanding of how to control and optimize quantum phenomena, highlighting the model's relevance for quantum information processing technologies.

Keywords: two two-level atoms, parity deformed-coherent states, population, entanglement, Fisher information, concurrence

1 Introduction

Quantum entanglement (QE) represents a form of nonlocal correlation that distinguishes quantum systems from classical ones, forming a cornerstone of quantum mechanics [1,2]. In recent decades, rapid advancements in technology have positioned QE as a vital resource underpinning a wide array of quantum technologies, including quantum metrology [3–5], quantum thermodynamics [6,7], and solid-state physics [8–12]. As a result, the precise characterization and quantification of QE have become a focal point of extensive research efforts [1,2,13]. Breakthroughs in quantum information technology have further enriched our understanding of nonlocal correlations, unveiling intricate phenomena such as the sudden birth and sudden death of QE [14,15]. However, despite its promising applications, the practical use of QE in quantum information processing is often hindered by decoherence, which can lead to the degradation of quantum correlations over time. This makes the study of QE's dynamical decay, stabilization, and protection mechanisms critically important for the advancement of robust quantum systems. Understanding these processes is crucial for maintaining QE in real-world applications, ensuring the long-term stability and efficiency of quantum technologies, and enhancing the resilience of quantum information against environmental perturbations. Such a system – two identical two-level atoms interacting with a parity-deformed coherent field under intensity-dependent coupling – offers a versatile platform for simulating nonclassical light–matter interactions, which are integral to quantum information tasks such as entanglement generation, quantum state control, and high-precision metrology.

Quantum Fisher Information (QFI) plays a crucial role in the parameter estimation theory, setting fundamental precision limits for quantum measurements [16]. As a key tool in quantum metrology, QFI has found applications in technologies such as quantum frequency standards [17], clock synchronization [16], and gravitational acceleration measurements [18]. It quantifies the statistical distinguishability of parameters encoded within quantum states and establishes the precision limit *via* the Cramér–Rao inequality, where QFI determines the lower bound of achievable variance in estimation [4,19,20]. The connection between QFI and QE is particularly profound; it has been shown that QFI provides a more stringent criterion for

*** Corresponding author: Sayed Abdel-Khalek,** Department of Mathematics and Statistics, College of Science, Taif University, P.O. Box 11099, Taif, 21944, Saudi Arabia, e-mail: sayedquantum@yahoo.co.uk
Mariam Algarni: Department of Mathematical Sciences, College of Science, Princess Nourah bint Abdulrahman University, P.O. Box 84428, Riyadh, 11671, Saudi Arabia
Kamal Berrada: Department of Physics, College of Science, Imam Mohammad Ibn Saud Islamic University (IMSIU), P.O. Box 90950, Riyadh, 11432, Saudi Arabia

detecting QE compared to spin squeezing, making it a more robust tool for assessing quantum correlations [21,22]. In open quantum systems, where interactions with the environment lead to decoherence, QFI becomes essential for estimating noise parameters in amplitude-damping [23,24] and depolarizing channels [25], helping to improve the resilience of quantum systems to environmental disturbances. Additionally, in bosonic channels, the use of Gaussian squeezed probes has demonstrated that QFI can significantly enhance the precision of loss parameter estimation, making it valuable for optimizing quantum communication and sensing technologies in lossy environments [26]. Recent advances have further expanded the use of QFI in studying quantum phase transitions, where it provides insights into critical phenomena and phase behavior in quantum systems [27,28]. By characterizing these transitions, QFI helps to identify and exploit quantum phases that are useful for enhancing the precision and robustness of quantum technologies. Thus, QFI not only defines fundamental limits of measurement precision but also serves as a versatile tool in understanding complex quantum dynamics, quantum correlations, and system–environment interactions.

The Jaynes–Cummings model (J-CM) is a cornerstone of quantum optics, providing a rigorous framework to describe the interaction between a two-level atom and a quantized electromagnetic field. This model has been instrumental in revealing fundamental quantum phenomena, including quantum revivals, collapses, atom-field entanglement, and Rabi oscillations [29,30]. In recent years, its significance has grown in the field of quantum information processing, where it is pivotal for the generation and manipulation of nonclassical states, which are essential for tasks such as quantum computing and secure communication [31]. The predictions of the J-CM have been experimentally validated through studies using Rydberg atoms in quantum electrodynamics cavities, demonstrating its robustness and applicability in real-world scenarios [32]. Moreover, the J-CM has been extended to explore more complex interactions, including multi-photon transitions and systems involving three- or four-level atoms in cavity fields. The Tavis–Cummings model further generalizes the J-CM by considering various atoms interacting with a single quantized field, thereby uncovering collective effects and phenomena such as superradiance [33,34]. Additionally, advancements in algebraic methods have led to the development of deformed versions of the J-CM, where ordinary creation and annihilation operators are replaced with deformed operators. This modification allows for the exploration of novel quantum dynamics and provides deeper insights into the behavior of systems under non-standard interactions, enhancing our understanding of the rich landscape of quantum phenomena [35,36].

In this work, we explore the dynamics of a two two-level atomic system (TTLA) interacting with a parity-deformed field, modeled as a coherent state (PD-CS). By varying the parity deformation parameter and incorporating the effects of intensity-dependent coupling (I-DC), we examine the time evolution of key quantum phenomena, considering atomic population inversion, von Neumann entropy, concurrence, quantum Fisher information, and the Mandel parameter, where each serves as a critical indicator. We show how the interplay between the deformation parameter and coupling effects governs the quantum dynamics, influencing entanglement, quantum Fisher information, and statistical properties of the field.

The remainder of this article is structured as follows: Section 2 provides a detailed physical description of the quantum system and its dynamics. In Section 3, we introduce and discuss the key quantifiers used in this study, including atomic population inversion, von Neumann entropy, concurrence, the QFI, and the Mandel parameter. The numerical results and the analysis of the quantifier are also presented. Finally, in Section 4, we summarize our findings and offer concluding remarks.

2 Theoretical model and description

The proposed quantum system consists of two identical two-level atoms exposed to a parity-deformed field (P-DF). This atomic system has many applications and may be useful in developing quantum information theory. Based on the rotating wave approximation, the interaction Hamiltonian that describes this system is written as (setting $\hbar = 1$):

$$\hat{H}_I = \mu \sum_{k=1}^{2} (\hat{A} G(\hat{A}^\dagger \hat{A}) |e_k\rangle\langle g_k| + G(\hat{A}^\dagger \hat{A}) \hat{A}^\dagger |g_k\rangle\langle e_k|), \quad (1)$$

where $\hat{A}(\hat{A}^\dagger)$ is the parity-deformed creation (annihilation) operator and has this action as $\hat{A}|2n\rangle = \sqrt{2n}\,|2n-1\rangle, \hat{A}^\dagger|2n\rangle = \sqrt{2n+2l+1}\,|2n+1\rangle$. Moreover, $|e_k\rangle(|g_k\rangle)$ corresponds to the upper (lower) state of each kth − TLA. Also, μ and $G(\hat{A}^\dagger \hat{A})$ indicate the constant and I-DC between the TTLA and P-DF. In this paper, we discuss two cases of $G(\hat{A}^\dagger \hat{A})$ as $G(\hat{A}^\dagger \hat{A}) = 1$ (slandered parity-deformed T-CM (absence of I-DC effect) and $G(\hat{A}^\dagger \hat{A}) = \sqrt{\hat{A}^\dagger \hat{A}}$ (presence of I-DC).

The coherent states related to the P-DF as an eigenstate of the square of the l–deformed annihilation operator $\hat{A}^2|\alpha\rangle_l = \alpha^2|\alpha\rangle_l$. In this way, the initial state of the P-DF is given by [37]

$$|\Psi_F(0)\rangle = \sqrt{\frac{|\alpha|^{2l-1}}{2^{l-\frac{1}{2}}I_{l-\frac{1}{2}}(|\alpha|^2)}}\sum_{m=0}^{\infty}\left(\frac{\alpha^{2m}}{2^m\sqrt{\Gamma(m+1)\Gamma\left(m+l+\frac{1}{2}\right)}}\right), \quad (2)$$

$$|2m\rangle = \sum_{m=0}^{\infty} \mathrm{D}_m(\ell)|2m\rangle$$

where $D_m(\ell) = \frac{|\alpha|^{2m+\ell-\frac{1}{2}}}{2^{m+\frac{\ell}{2}-\frac{1}{4}}\sqrt{I\left(\ell-\frac{1}{2},|\alpha|^2\right)\Gamma(m+1)\Gamma\left(m+\ell+\frac{1}{2}\right)}}$.

The TTLA–P-DF state vector at any time $t > 0$, can be formulated as

$$|\Psi_s(t)\rangle = \sum_{n=0}^{\infty} B_1(n,t)|2n, e_1e_2\rangle + B_2(n,t)|2n+1, e_1g_2\rangle + B_3(n,t)|2n+1, g_2e_1\rangle + B_4(n,t)|2n+2, g_2g_1\rangle. \quad (3)$$

Now, we suppose that at $t = 0$, the TTLA are initially prepared in the Bell states and the P-DF in the coherent state (5). The state vector at $t = 0$ is

$$|\Psi_s(0)\rangle = |\Psi_F(0)\rangle \otimes |\Psi_{TTLA}(0)\rangle = \sum_{m=0}^{\infty} \mathrm{D}_m(\ell)|2m\rangle \otimes \frac{1}{\sqrt{2}}(|e_1e_2\rangle + |g_1g_2\rangle), \quad (4)$$

The coefficients $B_j, j = 1, 2, 3, 4$, can be obtained by solving the Schrödinger equation

$$-i\frac{\partial}{\partial t}|\Psi_s(t)\rangle = \hat{H}_I|\Psi_s(t)\rangle, \quad (5)$$

The total density matrix corresponds to the atomic system $\rho_s(t) = |\Psi_s(t)\rangle\langle\Psi_s(t)|$. The reduced density matrix of the TTLA (P-DF) after taking the trace over P-DF (TTLA) can be obtained as

$$\rho_{TTLAs}(t) = \mathrm{Tr}_{P-DF}\{\rho_s(t)\} = \sum_{j=1}^{4}\sum_{r=1}^{4}\rho_{jr}\ |j\rangle\langle r|, \quad (6)$$

$$\rho_{P-DF}(t) = \mathrm{Tr}_{TQS}\{\rho_{TQS-F}(t)\} = \sum_{n=0}^{\infty}\rho_n\ |2n\rangle\langle 2n|. \quad (7)$$

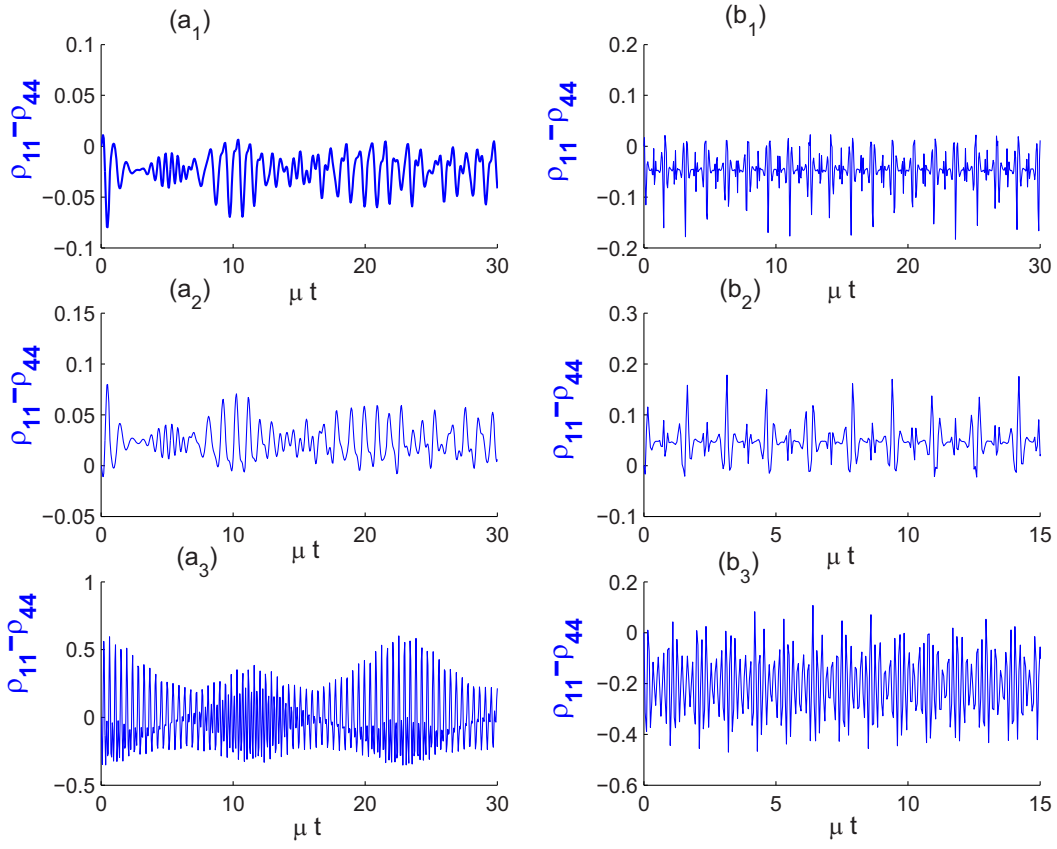

Figure 1: Time evolution of the atomic inversion ρ_z for the TTLA interacting with the P-DF for $\alpha = \sqrt{5}$. Panels ($a_j, j = 1, 2, 3$) corresponding to $G(A^+A) = 1$ (absence of the I-DC effect) and (b_j) for $G(A^+A) = \sqrt{A^+A}$ (presence of the I-DC effect). Also, with various values of the P-DF parameter ℓ as $\ell = 0$, 1, and 50 correspond to, respectively, panels (a_1, b_1), (a_2, b_2), and (a_3, b_3).

Next, we shall consider the effect of the t-dc and P-DF on the dynamical properties of the atomic inversion, TLA-TLA, TTLA-P-DF entanglement, and the QFI. The photon statistics of the field with be investigated *via* the evolution of the Mandel parameter.

3 Quantum measures and numerical results

Here, we define the different measures of entanglement measuring quantifiers and discuss their behavior with respect to t-dc and P-DF effects.

3.1 Atomic inversion

In the context of quantum optics, atomic inversion is used for identifying the periods of collapse and revival, which are essential for determining the intervals during which the atomic system exhibits maximal entanglement or separability. Atomic inversion is defined by the difference between the diagonal elements of the TTLA density matrix (6), specifically as

$$\begin{aligned}\rho_z(t) &= \rho_{11}(t) - \rho_{44}(t)\\ &= \sum_{m=0}^{\infty} (\lceil R_1(2m,t)\rceil^2 - \lceil R_4(2m,t)\rceil^2).\end{aligned} \tag{8}$$

Figure 1 illustrates the dynamics of atomic population for a TTLA interacting with a PD-CS for $\alpha = \sqrt{5}$. Panels (a_1), (a_2), and (a_3) depict the behavior of the TTLA with I-DC under varying values of the parity-deformed parameter $l = 0, 1$, and 50, respectively. For $l = 0$, the atomic population inversion exhibits oscillatory behavior with notable packet-like revivals characterized by an increasing amplitude that dissipates over time. The population is unevenly distributed along the line $\rho_z = 0$ line, with most dynamics concentrated below this line. As l increases to 1, the system continues to show oscillatory dynamics with revival-like behavior. However, compared to the $l = 0$ case, the population dynamics shift predominantly above the line $\rho_z = 0$,

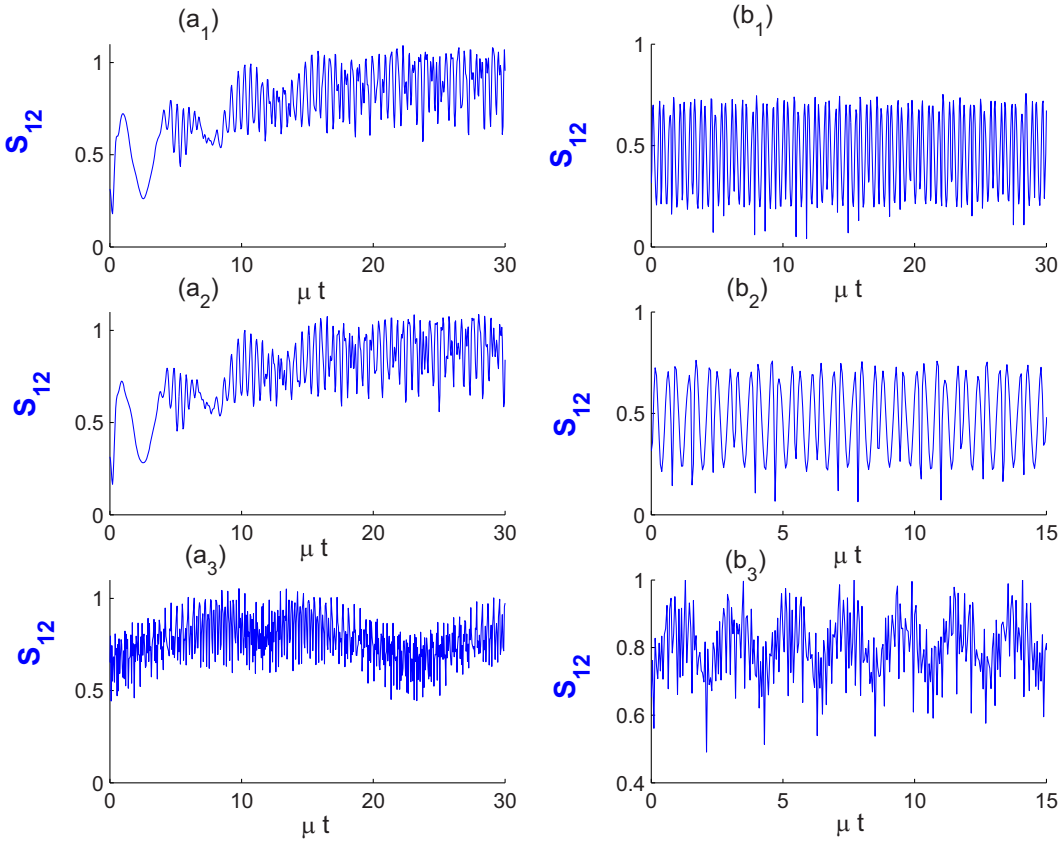

Figure 2: Time evolution of the von Neumann entropy S_{12} for the TTLA interacting with the P-DF for $\alpha = \sqrt{5}$. Panels ($a_j, j = 1, 2, 3$) corresponding to $G(A^+A) = 1$ (absence of the I-DC effect) and (b_j) for $G(A^+A) = \sqrt{A^+A}$ (presence of the I-DC effect). Also, with various values of the P-DF parameter ℓ as $\ell = 0, 1$, and 50 correspond to, respectively, panels (a_1, b_1), (a_2, b_2), and (a_3, b_3).

while still remaining unevenly distributed. When $l = 50$, oscillations become more rapid, and the atomic population increasingly favors positive values of ρ_z. The revival packets grow larger, highlighting a stark contrast to the lower l values. Panels (b_1), (b_2), and (b_3) present the atomic population dynamics with I-DC effects for $l = 0, 1$, and 50, respectively. In panel (b_1), corresponding to $l = 0$, revivals are more pronounced compared to the scenario without I-DC, with the population remaining predominantly below the line $\rho_z = 0$ and lacking distinct packet-like revivals. For $l = 1$ (panel b_2), the dynamics exhibit population revivals mostly above the line $\rho_z = 0$, with brief intervals of collapse similar to the $l = 0$ case. Finally, in panel (b_3) for $l = 50$, rapid oscillations are observed alongside packet-like revivals. The amplitude of these revivals is slightly increased, with population dynamics now primarily occurring below the line $\rho_z = 0$, contrasting with the scenario without I-DC. The revival patterns observed in atomic population inversion indicate controllable periodic exchange of energy between the atoms and the field, which is critical for synchronizing atomic states in quantum memories or processors.

3.2 TTLA–P-DF entanglement

The entanglement between the P-DF and TTLA can be inferred from the evolution of the subsystem's von Neumann entropy. It is defined in terms of the TTLA density matrix as

$$S_{12} = -\mathrm{Tr}\{\rho_{\mathrm{TTLAs}}(t)\ln[\rho_{\mathrm{TTLAs}}(t)]\}. \tag{9}$$

Here, ρ_{TTLAs} represents the TTLA density operator as defined in Eq. (6). The von Neumann entropy S_{12} is given by

$$S_{\mathrm{F-LA}} = -\sum_{j=1}^{4} c_j \ln c_j, \tag{10}$$

where c_j is the jth eigenvalue of ρ_{TTLAs}.

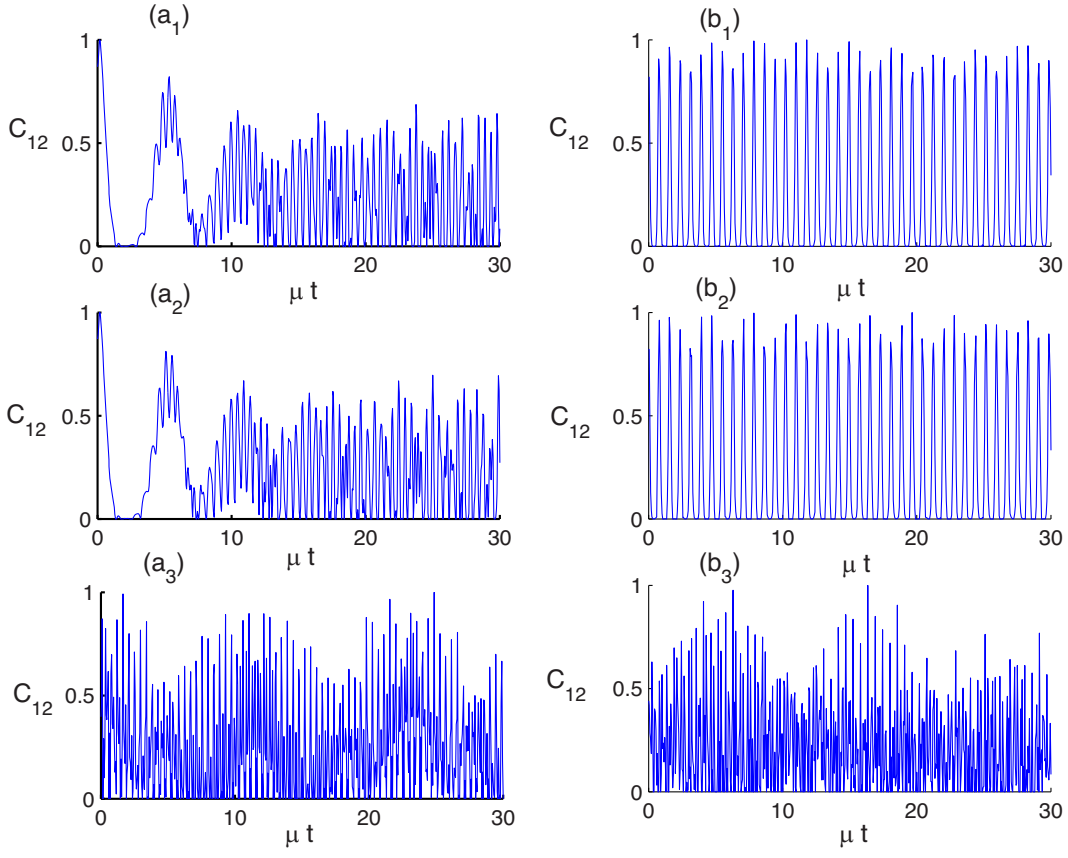

Figure 3: Time evolution of the concurrence C_{12} for the TTLA interacting with the P-DF for $\alpha = \sqrt{5}$. Panels (a_j, $j = 1, 2, 3$) corresponding to $G(A^+A) = 1$ (absence of the I-DC effect) and (b_j) for $G(A^+A) = \sqrt{A^+A}$ (presence of the I-DC effect). Also, with various values of the P-DF parameter ℓ as $\ell = 0, 1$, and 50 corresponds to, respectively, panels (a_1, b_1), (a_2, b_2), and (a_3, b_3).

Figure 2 displays the evolution of the von Neumann entropy for a TTLA interacting with a PD-CS for $\alpha = \sqrt{5}$. The analysis considers varying the parity-deformed parameter $l = 0, 1$, and 50 under both I-D and non-I-DC scenarios. In the absence of I-DC, subplots (a_1), (a_2), and (a_3) illustrate the dynamics for increasing values of l. For $l = 0$, the von Neumann entropy exhibits oscillatory behavior that initially increases and ultimately settles into a steady-state oscillation around a specific value, with the amplitude of oscillations growing over time. For $l = 1$, a similar pattern is observed, with increasing oscillations stabilizing around a steady-state value as time progresses. At $l = 50$, the dynamics become more rapid, with oscillations fluctuating around a constant value, while the amplitude remains unchanged over time. When I-DC is introduced, as shown in subplots (b_1), (b_2), and (b_3), the von Neumann entropy displays rapid oscillatory behavior for both $l = 0$ and $l = 1$. In these cases, the oscillations center around a value of approximately 0.5, maintaining a consistent amplitude throughout the dynamics. For $l = 50$, the von Neumann entropy continues to exhibit rapid and periodic oscillations; however, the central value around which the system fluctuates shifts to approximately $S_{12} = 0.8$, which is higher compared to the $l = 0$ and $l = 1$ cases, where S_{12} remains around 0.5.

3.3 TLA–TLA entanglement

Here, we use the concurrence to measure TLA–TLA entanglement [38]. It is defined as

$$C_{12} = \max\{0, \beta_1 - \beta_2 - \beta_3 - \beta_4\}, \tag{11}$$

where β_j defines the eigenvalues given in decreasing order of the matrix $\boldsymbol{\rho}_{\mathbf{TTLAs}}\tilde{\rho}_{\mathrm{TTLA}}$s, where $\tilde{\rho}_{\mathbf{TTLAs}}$ is the density matrix related to the Pauli matrix σ_Y and ρ^*_{TQS} (complex conjugate of $\boldsymbol{\rho}_{\mathbf{TTLAs}}$) by

$$\tilde{\rho}_{\mathbf{TTLAs}} = (\sigma_Y \otimes \sigma_Y)\rho^*_{\mathrm{TTLA}}(\sigma_Y \otimes \sigma_Y), \tag{12}$$

where C_{12} has zero value for the TTLA is in a separable state, and it reaches to its maximum value $C_{12} = 1$ for the TTLA in the maximally entangled state.

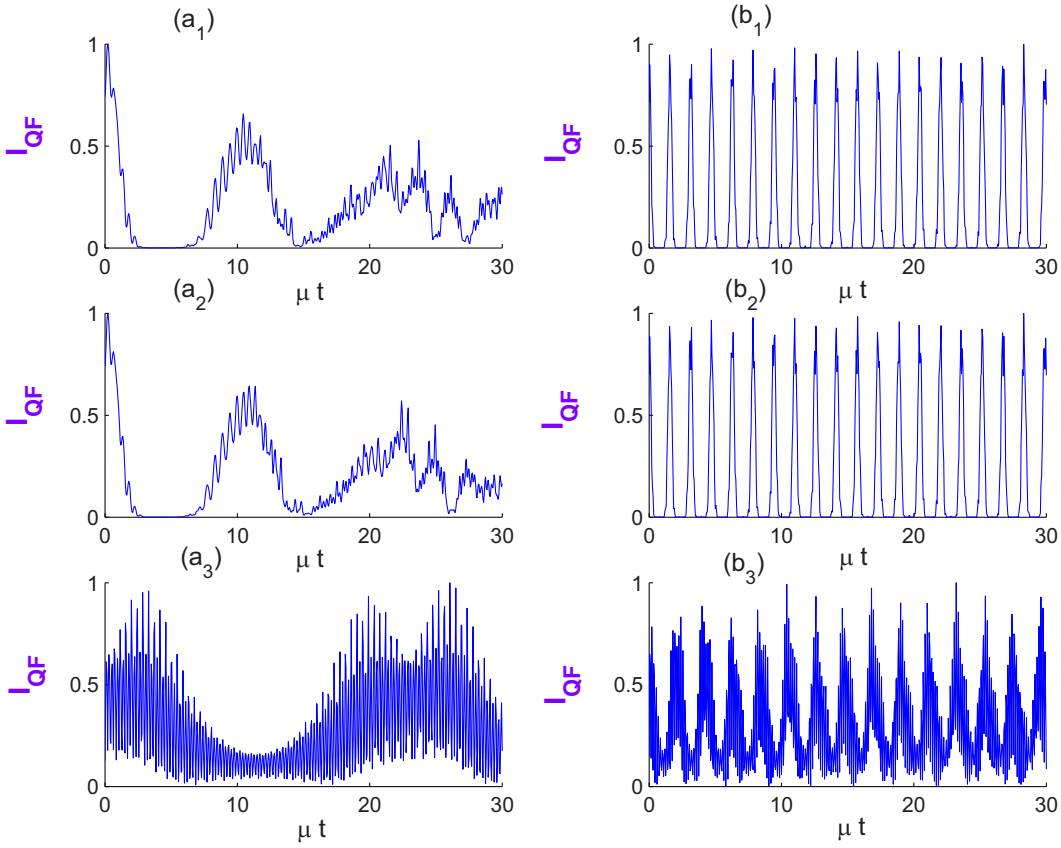

Figure 4: Evolution of the QFI I_{QF} for the TTLA interacting with the P-DF for $\alpha = \sqrt{5}$. Panels $(\mathrm{a}_j, j = 1, 2, 3)$ corresponding to $G(A^+A) = 1$ (absence of the I-DC effect) and (b_j) for $G(A^+A) = \sqrt{A^+A}$ (presence of the I-DC effect). Also, with various values of the P-DF parameter ℓ as $\ell = 0, 1$, and 50 corresponds to, respectively, panels $(\mathrm{a}_1, \mathrm{b}_1)$, $(\mathrm{a}_2, \mathrm{b}_2)$, and $(\mathrm{a}_3, \mathrm{b}_3)$.

Figure 3 illustrates the time evolution of the concurrence C_{12} for a TTLA interacting with a parity-deformed coherent field, considering varying deformed parameters $l = 0, 1$, and 50. The analysis addresses both scenarios: without and with I-DC. In the absence of I-DC, as shown in subplots (a_1), (a_2), and (a_3), the concurrence dynamics evolve as follows: for =0 and $l = 1$, C_{12} starts at 1 and gradually decreases. Initially, the dynamics lack oscillations, but as time progresses, rapid oscillations emerge, eventually stabilizing into a nearly constant amplitude. When the deformed parameter is increased to $l = 50$, the dynamics exhibit rapid and periodic oscillations, with the amplitude of these oscillations varying periodically over time. When I-DC is introduced, as depicted in subplots (b_1), (b_2), and (b_3), the concurrence C_{12} displays oscillatory behavior within the range of 0–1. The period of oscillation remains consistent for both $l = 0$ and $l = 1$, with the amplitude showing a slight sinusoidal variation throughout the evolution. For $l = 50$, the dynamics reveal even more rapid oscillations, with the period of oscillation increasing compared to the lower l values. The amplitude of these oscillations forms revival packets, adding complexity to the overall behavior. The steady-state oscillations in von Neumann entropy and concurrence under certain parameters highlight entanglement stabilization regimes, which are useful in maintaining coherence during information processing.

3.4 QEI dynamics

The quantum version of QFI concerning the estimation parameter φ can be investigated through the symmetric logarithmic derivative $\wp(\varphi, t)$ as outlined in [39,40]

$$I_{\mathrm{QF}} = \mathrm{Tr}[\hat{\rho}_{\mathrm{TTLAs}}\wp^2], \tag{13}$$

with

$$\frac{\partial\hat{\rho}_{\mathrm{TTLAs}}}{\partial\varphi} = \frac{1}{2}(\hat{\rho}_{\mathrm{TTLAs}}\wp(\varphi, t) + \wp(\varphi, t)\hat{\rho}_{\mathrm{TTLAs}}), \tag{14}$$

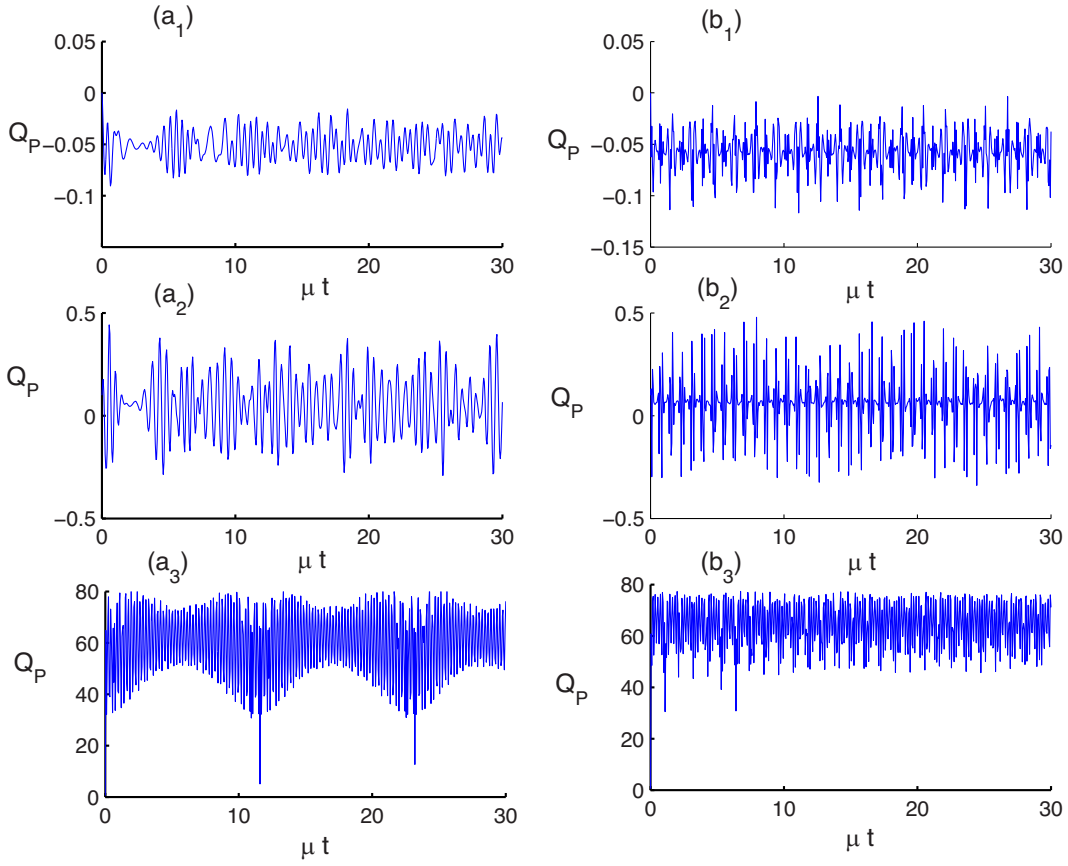

Figure 5: Time evolution of the Mandel parameter Q_{P} for the TTLA interacting with the field in the PD-CS for $\alpha = \sqrt{5}$. Panels ($a_j, j = 1, 2, 3$) corresponding to the absence of the I-DC effect (*i.e.* $G(A^{+}A) = 1$) and ($b_j, j = 1, 2, 3$) are plotted under the effect of I-DC for $G(A^{+}A) = \sqrt{A^{+}A}$ and with different values of the parity-deformed parameter ℓ as $\ell = 0, 1$, and 50 in panels (a_1, b_1), (a_2, b_2), and (a_3, b_3).

Figure 4 illustrates the dynamics of the QFI for a two-level atomic system TTLA interacting with a PD-CS under varying parity-deformed parameters $l = 0, 1$, and 50. The analysis encompasses both scenarios: with and without I-DC effects. In the absence of I-DC, subplots (a_1), (a_2), and (a_3) demonstrate the impact of the deformed parameter l on the QFI dynamics. For $l = 0$ and $l = 1$, the QFI initially starts at a value of 1 and subsequently exhibits a decaying behavior over time. This decay is accompanied by oscillations that vary in amplitude as the system evolves. As the parity-deformed parameter increases to $l = 50$, the dynamics become more complex, characterized by rapid oscillations with significantly higher amplitude than in the $l = 0$ and $l = 1$ cases. Notably, the QFI does not consistently decrease; instead, rapid oscillations periodically decay and revive within the observed time scale. When I-DC is introduced, as shown in subplots (b_1), (b_2), and (b_3), the QFI dynamics change significantly. For $l = 0$ and $l = 1$, the QFI exhibits periodic revivals punctuated by brief intervals of collapse. The period of oscillation remains consistent across both values of the parity-deformed parameter, though the amplitude varies throughout the dynamics. For $l = 50$, the system displays rapid oscillatory behavior, with revivals manifesting as rapid oscillation packets. The amplitude of these oscillations shows a slight decrease compared to the cases with $l = 0$ and $l = 1$, adding subtle complexity to the overall dynamics. Fluctuations in quantum Fisher information reveal periods of enhanced parameter sensitivity, making the system viable for quantum sensing and clock synchronization.

3.5 Field photon statistics

We use the Mandel parameter to examine the nonclassical properties and photon distribution in the P-DF. This parameter is defined as [41]

$$Q_{\mathrm{P}} = \frac{\mathrm{Tr}(\hat{A}^{\dagger}\hat{A})^2}{\mathrm{Tr}(\mathrm{A}^{\dagger}\hat{A})} - \mathrm{Tr}(\mathrm{A}^{\dagger}\hat{A}) - 1, \tag{15}$$

The field is governed by super-Poissonian statistics for $Q_{\mathrm{P}} > 0$, Poissonian statistics for $Q_{\mathrm{P}} = 0$, and sub-Poissonian statistics for $Q_{\mathrm{P}} < 0$, which indicates that photons are anti-bunched. The sub-Poissonian statistics indicates that the field has a quantum nature.

Figure 5 presents the time evolution of the Mandel parameter Q_{p} for a system interacting with a parity-deformed coherent state under varying values of the parity-deformed parameter $l = 0, 1$, and 50. The analysis considers two scenarios: with and without the I-DC effects. In the absence of I-DC, subplots (a_1), (a_2), and (a_3) depict the dynamics of the Mandel parameter for different values of l. For $l = 0$, the dynamics exhibit oscillatory behavior characterized by revival packets that gradually dissipate over time. The oscillations of the Mandel parameter occur predominantly below the $Q_{\mathrm{p}} = 0$. When $l = 1$, the dynamics show both collapses and revivals, beginning with an initial collapse in the Mandel parameter, followed by increased revival amplitudes as time progresses. These revivals are asymmetrically distributed around the line$Q_{\mathrm{p}} = 0$, tending more toward positive values. For $l = 50$, the dynamics become more rapid and periodic, with significantly increased oscillation amplitudes compared to the $l = 0$ and $l = 1$ cases. The amplitude of these oscillations varies periodically over time. Overall, the behavior of the Mandel parameter is highly dependent on the value of l, with both amplitude and frequency of oscillations increasing as l increases. When I-DC is introduced, as shown in subplots (b_1), (b_2), and (b_3), the dynamics of the Mandel parameter change notably. For $l = 0$, the Mandel parameter exhibits rapid oscillations, predominantly below the line $Q_{\mathrm{p}} = 0$, oscillating around $Q_{\mathrm{p}} = -0.05$. As l increases to 1, the Mandel parameter continues to show oscillatory behavior, now oscillating above the line $Q_{\mathrm{p}} = 0$, with revival amplitudes higher than in the $l = 0$ case. For $l = 50$, the dynamics exhibit even more rapid oscillations, with the amplitude of these oscillations remaining approximately constant but significantly enhanced compared to the lower l values. This indicates that the Mandel parameter is sensitive to the parity-deformed parameter l under I-DC. The amplitude of oscillations remains nearly constant in the presence of I-DC, whereas in the absence of such coupling, the amplitude varies periodically. Transitions between sub- and super-Poissonian statistics in the Mandel parameter mark nonclassical field properties, which are pivotal for low-noise quantum communication.

Recent studies [42–44] have emphasized the need for tunable entanglement and phase sensitivity in multi-level systems, reinforcing the relevance of intensity-dependent coupling and algebraic deformations, as explored in our work.

4 Conclusions

In summary, we have studied the dynamics of a TTLA interacting with a PD-CS. By varying the parity deformation parameter and incorporating the effects of I-DC, we have examined the time evolution of key quantum phenomena, including atomic population inversion, von Neumann entropy, concurrence, quantum Fisher information, and the Mandel parameter. Each of these indicators plays a crucial

role in understanding the underlying quantum dynamics. Our findings demonstrate how the interplay between the deformation parameter and coupling effects governs the quantum behavior of the system. Specifically, we observed that variations in the parity deformation parameter significantly influence entanglement dynamics, parameter estimation capabilities, and the statistical properties of the field. For instance, as the deformation parameter increases, we noted enhanced oscillatory behaviors and revival characteristics that suggest a rich landscape of quantum effects that can be manipulated. These findings enhance our understanding of how to manage and refine quantum phenomena, which is crucial for the progress of quantum information processing technologies. The outcomes highlight the possible applications of our model in fields like quantum communication, quantum cryptography, and quantum computing, where the precise manipulation of quantum states and resources is vital. Ultimately, this research provides a foundation for future investigations that will delve into additional parameters and coupling scenarios, thereby deepening our comprehension of quantum systems and their real-world applications.

Acknowledgments: The authors acknowledge to Princess Nourah bint Abdulrahman University Researchers Supporting Project number (PNURSP2025R225), Princess Nourah bint Abdulrahman University, Riyadh, Saudi Arabia.

Funding information: Princess Nourah bint Abdulrahman University Researchers Supporting Project number (PNURSP2025R225), Princess Nourah bint Abdulrahman University, Riyadh, Saudi Arabia.

Author contributions: All authors have accepted responsibility for the entire content of this manuscript and approved its submission.

Conflict of interest: The authors state no conflict of interest.

Data availability statement: All data generated or analyzed during this study are included in this published article.

References

[1] Horodecki R, Horodecki P, Horodecki M, Horodecki K. Quantum entanglement. Rev Mod Phys. 2009;81:865–942.
[2] Gühne O, Tóth G. Entanglement detection. Phys Rep. 2009;474(1–6):1–75.
[3] Giovannetti V, Lloyd S, Maccone L. Quantum-enhanced measurements: Beating the standard quantum limit. Science. 2004;306(5700):1330–6.
[4] Paris MGA. Quantum estimation for quantum technology. Int J Quantum Inf. 2009;7(Suppl 1):101–10.
[5] Caves CM. Quantum-mechanical noise in an interferometer. Phys Rev D. 1981;23(8):1693–708.
[6] Goold J, Huber M, Riera A, del Rio L, Skrzypczyk P. The role of quantum information in thermodynamics – a topical review. J Phys A: Math Theor. 2016;49(14):143001.
[7] Uzdin R, Levy A, Kosloff R. Equivalence of quantum heat machines, and quantum-thermodynamic signatures. Phys Rev X. 2015;5(3):031044.
[8] Loss D, DiVincenzo DP. Quantum computation with quantum dots. Phys Rev A. 1998;57(1):120–6.
[9] Kane BE. A silicon-based nuclear spin quantum computer. Nature. 1998;393(6681):133–7.
[10] Imamoglu A, Awschalom DD, Burkard G, DiVincenzo DP, Loss D, Sherwin M, et al. Quantum information processing using quantum dot spins and cavity QED. Phys Rev Lett. 1999;83(20):4204–7.
[11] Petta JR, Johnson AC, Taylor JM, Laird EA, Yacoby A, Lukin MD, et al. Coherent manipulation of coupled electron spins in semiconductor quantum dots. Science. 2005;309(5744):2180–4.
[12] Greentree AD, Tahan C, Cole JH, Hollenberg LCL. Quantum phase transitions of light. Nat Phys. 2006;2(12):856–61.
[13] Amico L, Fazio R, Osterloh A, Vedral V. Entanglement in many-body systems. Rev Mod Phys. 2008;80(2):517–76.
[14] Yu T, Eberly JH. Sudden death of entanglement. Science. 2009;323(5914):598–601.
[15] Nielsen MA, Chuang IL. Quantum computation and quantum information. United Kingdom: Cambridge University Press; 2010.
[16] Giovannetti V, Lloyd S, Maccone L. Quantum metrology. Phys Rev Lett. 2006;96(1):010401.
[17] Pezze L, Smerzi A. Quantum theory of phase estimation. Arimondo E, Ertmer W, Schleich W, editors. In Atom interferometry. Vol. 188, Amsterdam: IOS Press; 2009. p. 691–741.
[18] Bize S, Laurent P, Abgrall M, Marion H, Maksimovic I, Cacciapuoti L, et al. Cold atom clocks and applications. J Phys B: Mol Opt Phys. 2005;38(9):S449–68.
[19] Braunstein SL, Caves CM. Statistical distance and the geometry of quantum states. Phys Rev Lett. 1994;72(22):3439–43.
[20] Holevo AS. Probabilistic and statistical aspects of quantum theory. Amsterdam: North-Holland Publishing Co.; 1982.
[21] Pezze L, Smerzi A. Entanglement, nonlinear dynamics, and the Heisenberg limit. Phys Rev Lett. 2009;102(10):100401.
[22] Wang X, Sanders BC. Spin squeezing and pairwise entanglement for symmetric multiqubit states. Phys Rev A. 2003;68(1):012101.
[23] Demkowicz-Dobrzański R, Dorner U, Smith BJ, Lundeen JS, Wasilewski W, Banaszek K, et al. Quantum phase estimation with lossy interferometers. Phys Rev A. 2009;80(1):013825.
[24] Fujiwara A. Estimation of a noise parameter in quantum two-level systems. Phys Rev A. 2001;63(4):042304.
[25] Macchiavello C, Palma GM. Entanglement-enhanced information transmission over a quantum channel with correlated noise. Phys Rev A. 2002;65(5):050301.
[26] Aasi J, Abadie J, Abbott BP, Abbott R, Abbott TD, Abernathy MR, et al. Enhanced sensitivity of the LIGO gravitational wave detector by using squeezed states of light. Nat Photon. 2013;7(8):613–9.

[27] Quan HT, Song Z, Liu XF, Zanardi P, Sun CP. Decay of Loschmidt Echo enhanced by quantum criticality. Phys Rev Lett. 2006;96(14):140604.
[28] Venuti LC, Zanardi P. Quantum critical scaling of the geometric tensors. Phys Rev Lett. 2007;99(9):095701.
[29] Jaynes ET, Cummings FW. Comparison of quantum and semiclassical radiation theories with application to the beam maser. Proc IEEE. 1963;51(1):89–109.
[30] Brune M, Schmidt-Kaler F, Maali A, Dreyer J, Hagley E, Raimond JM, et al. Quantum Rabi oscillation: A direct test of field quantization in a cavity. Phys Rev Lett. 1996;76(11):1800–3.
[31] Zheng SB, Guo GC. Efficient scheme for two-atom entanglement and quantum information processing in cavity QED. Phys Rev Lett. 2000;85(11):2392–5.
[32] Kuang LM, Zhou L. Two-mode multiphoton Jaynes-Cummings model: Dynamics of entanglement and quantum collapse and revival. Phys Rev A. 2003;68(4):043606.
[33] Arecchi FT, Courtens E. Experimental study of Rabi oscillations in a spin-resonance experiment. Phys Rev Lett. 1972;29(6):409–12.
[34] Chaichian M, Ellinas D, Kulish P. Quantum algebra as the dynamical symmetry of the deformed Jaynes-Cummings model. Phys Rev Lett. 1990;65(8):980–3.
[35] Nieto MM. Quantum-deformed creation and annihilation operators. Phys Lett A. 1997;229(3):135–42.
[36] Roy B, Roy P. Deformed Jaynes-Cummings model with a q-deformed field. J Opt B: Quantum Semiclassical Opt. 2000;2(1):65–8.
[37] Dehghani A, Mojaveri B, Shirin S, Amiri Faseghandis S,. Parity deformed Jaynes-Cummings model: Robust maximally entangled states. Sci Rep. 2016;6:38069.
[38] Wootters WK. Entanglement of formation and concurrence. Quantum Inf Comput. 2001;1:27.
[39] Fisher RA. Bennett JH, editor. Proc. Cambridge Phil. Soc. 1929, 22, 700 reprinted in Collected Papers of R. A. Fisher. South Australia: Univ. of Adelaide Press; 1972. p. 15–40.
[40] Barndorff-Nielsen OE, Gill RD, Jupp PE. On quantum statistical inference. J R Stat Soc B. 2003;65:775.
[41] Mandel L, Wolf E. Optical coherent and quantum optics. United Kingdom: Cambridge University Press; 1955.
[42] Baksic A, Cristiano C. Controlling discrete and continuous symmetries in superconducting qubits. Phys Rev Lett. 2019;123:260402.
[43] Ding CY, Ji LN, Chen T, Xue ZY. Path-optimized nonadiabatic geometric quantum computation on superconducting qubits. Quantum Sci Technol. 2022;7(1):015012.
[44] Liao Z, Zubairy MS. Controllable entanglement in atom–field systems. Opt Express, 2021;29:16428.